

# Probing the band structure of quadri-layer graphene with magneto-phonon resonance

C. Faugeras<sup>1</sup>, P Kossacki<sup>1, 2</sup>, A.A.L. Nicolet<sup>1</sup>, M. Orlita<sup>1</sup>, M Potemski<sup>1</sup>, A. Mahmood<sup>3</sup>, D.M. Basko<sup>4</sup>

<sup>1</sup> LNCMI-CNRS (UJF, UPS, INSA), BP 166, 38042 Grenoble Cedex 9, France

<sup>2</sup> Institute of Experimental Physics, University of Warsaw, Hoza 69, 00-681 Warsaw, Poland

<sup>3</sup> CNRS-Institut Néel, BP 166, 38042 Grenoble Cedex 9, France

<sup>4</sup> Université Grenoble 1/CNRS, LPMMC UMR 5493, 25 rue des Martyrs, 38042 Grenoble, France

E-mail: clement.faugeras@lncmi.cnrs.fr

**Abstract.** We show how the magneto-phonon resonance, particularly pronounced in  $sp^2$  carbon allotropes, can be used as a tool to probe the band structure of multilayer graphene specimens. Even when electronic excitations cannot be directly observed, their coupling to the  $E_{2g}$  phonon leads to pronounced oscillations of the phonon feature observed through Raman scattering experiments with multiple periods and amplitudes determined by the electronic excitation spectrum. Such experiment and analysis have been performed up to 28T on an exfoliated 4-layer graphene specimen deposited on  $SiO_2$ , and the observed oscillations correspond to the specific AB stacked 4-layer graphene electronic excitation spectrum.

PACS numbers: 73.22.Lp, 63.20.Kd, 78.30.Na, 78.67.-n

Submitted to: *New J. Phys.*

## 1. Introduction

Since the theoretical prediction of magneto-phonon resonance in graphene and bilayer graphene [1, 2, 3], the resonant interaction between inter-Landau level electronic excitations and  $\Gamma$ -point optical phonon in graphene, this effect has been widely explored experimentally in neutral graphene-like systems such as multi layer epitaxial graphene on C-face SiC [4], graphene like inclusions on the surface of bulk graphite [5, 6], and in bulk graphite [7, 8]. Magneto-phonon resonance in these systems are pronounced because (i) they are gapless and low energy direct ( $\Delta k = 0$ ) electronic excitations exist, and (ii) because of the Kohn anomaly [9, 10] at the  $\Gamma$  point of the phonon Brillouin zone which makes phonon energies *ultra sensitive* to modifications of the electronic excitation spectrum. Such modifications can be achieved by tuning the Fermi energy or by applying a magnetic field perpendicular to the plane of the quasi-2D crystal.

Performed in systems with a well-known electronic excitation spectrum, magneto-phonon resonance experiments provide precise information concerning the electron-phonon interaction through the amplitude of the observed oscillations of the energy and of the line width of the phonon feature observed in Raman scattering experiments, as a function of the applied magnetic field. On the other hand, since electronic excitations which couple to the  $E_{2g}$  optical phonons are well identified by symmetry arguments (optical-like excitations characterized by a change of angular momentum  $\Delta|n| = \pm 1$  [1], where  $n$  is the Landau level index), this effect can be used to determine the electronic excitation spectrum. The evolution of optical-like excitations, calculated in the frame of Ref. [11], as a function of the magnetic field is presented in figure 1 for a) graphene, b) bilayer graphene, c) tri-layer graphene and d) for four-layer graphene. Each of these distinct electronic excitation spectra are tuned in resonance with the phonon energy at different characteristic values of the magnetic field. In analogy to magneto-transport experiments which probe the density of states at the Fermi energy, magneto-phonon resonance can be used as a probe of  $\Delta|n| = \pm 1$  electronic excitation at the  $E_{2g}$  phonon energy, and Landau level spectroscopy can be achieved by modelling the observed shifts of the phonon feature.

In this paper, we report on low-temperature magneto-Raman scattering experiments revealing the magneto-phonon resonance of an exfoliated multi-layer graphene specimen deposited on a  $\text{SiO}_2/\text{Si}$  substrate. The investigated sample is characterized by a low “intrinsic” doping and oscillations of both the phonon energy and line width can be observed for magnetic fields  $B > 7$  T. These oscillations have a noticeably more complicated pattern than for monolayer graphene and for bulk graphite. From the analysis of this pattern we deduce the number of layers in the sample, which turns out to be equal to four. Observation of a magneto-phonon resonance can hence be used to trace electronic excitations at the phonon energy and determine the band structure of the probed electronic system.

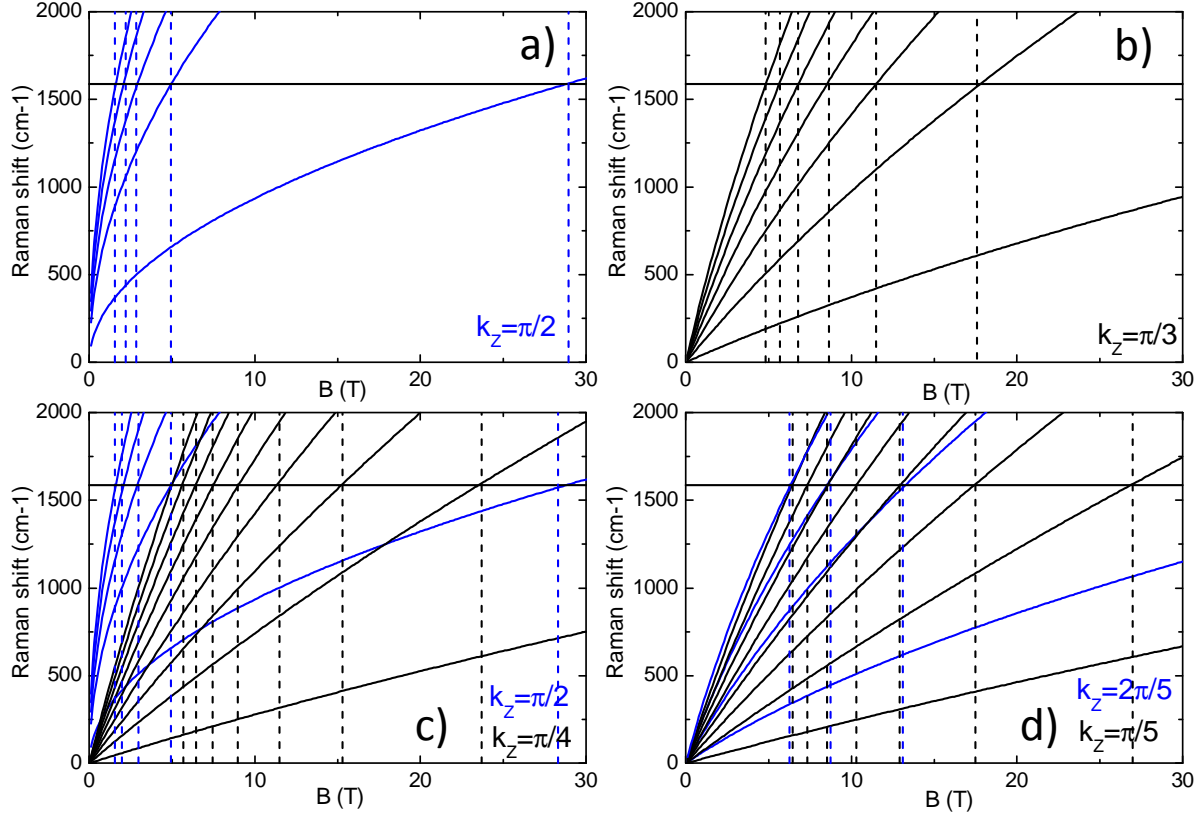


**Figure 1.** Evolution of inter Landau level excitations with  $\Delta|n| = \pm 1$  calculated in the frame of the model developed in Ref. [11], in the case of (a) a monolayer graphene, (b) a bilayer graphene, (c) a trilayer graphene and (d) four-layer graphene. The values of  $k_z$  used in these calculations are indicated in the figures. The phonon energy is indicated by the solid horizontal line at  $1585 \text{ cm}^{-1}$ . Dashed vertical lines indicate resonant magnetic fields corresponding to the different excitation spectra. Colors are only used to differentiate the different excitation spectra.

## 2. Experimental details

The multilayer graphene specimen is presented in the inset of figure 2a. It has been exfoliated from bulk graphite and deposited on a Si/SiO<sub>2</sub> substrate with 300 nm of SiO<sub>2</sub>. A single metallic electrode was then deposited on the flake (not used in this experiment). To locate the sample, we spatially map the Raman scattering signal of the silicon substrate, which shows a strong attenuation when the laser spot is focused on the metallic layer. A typical room temperature Raman scattering spectrum of the multilayer graphene flake measured with LABRAM confocal micro-Raman scattering set-up, together with an optical image are presented in figure 2a. The 2D band has a multi-components broad feature. We find the standard analysis of 2D band features in multi-layers specimens, that is, the deconvolution of the complex 2D band line shape using  $2N$  Lorentzian functions (where  $N > 1$  is the number of layers), relevant for mono-layers, for bi-layers and for tri-layers [12, 13, 14], not precise enough for  $N > 3$ . As a consequence, 4-layer graphene flakes can hardly be distinguished from the 5-layer

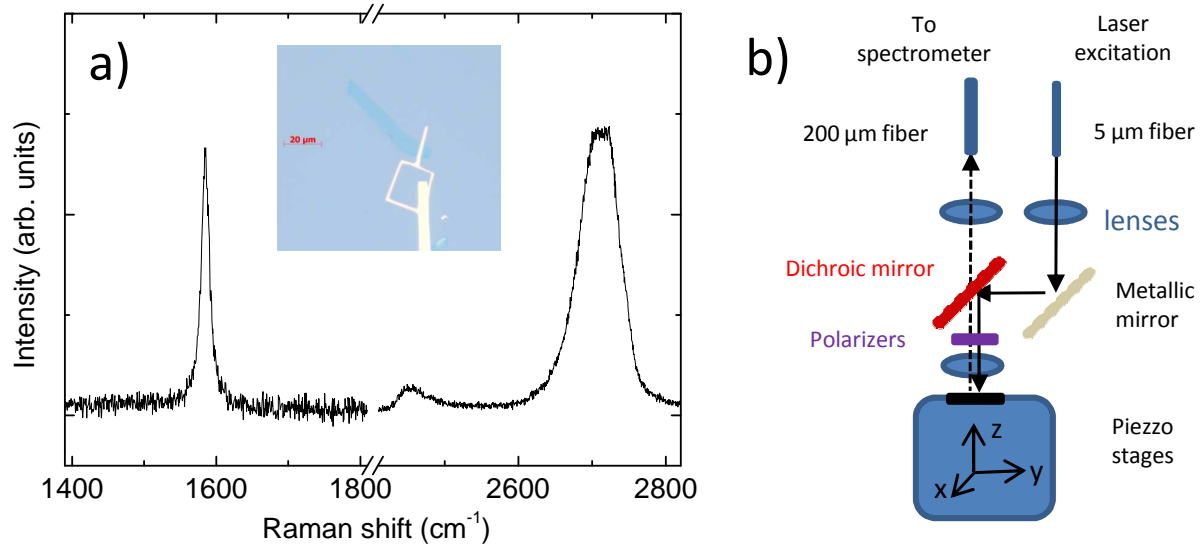


**Figure 2.** a) Raman scattering spectrum of the four-layer graphene specimen measured at room temperature with a LABRAM confocal micro-Raman scattering set-up, with the  $\lambda = 514.5$  nm line of an argon laser. Inset: Microscope image of the 4-layer graphene flake. b) Schematics of the micro-Raman scattering set-up operating at liquid helium temperature and in high magnetic fields.

and additional information is needed to fully characterized multilayer graphene systems.

The low-temperature magneto-Raman scattering response of our multilayer graphene has been measured with a home-made micro-Raman scattering setup presented in figure 2b. Laser excitation at  $\lambda = 488$  nm produced by an Ar ion laser is injected into a  $5 \mu\text{m}$  core mono-mode optical fiber which is fixed on a miniaturized optical bench and placed at the center of the magnet. This experimental setup can host various optical filters which are used to filter the excitation laser light at the output of the mono mode fiber (laser line filter), to selectively reflect the excitation laser and transmit the scattered signal (dichroic mirror), to reject the scattered laser before the collection fiber (notch filter), and to impose a circular polarization (linear polarizers and quarter wave plate). The excitation spot on the surface of the sample has a diameter of  $\sim 1 \mu\text{m}$  and the optical power is of 5 mW. The sample is mounted on piezo stages which allow to move the sample under the laser spot with a sub-micrometer resolution. Polarized Raman scattering spectra were measured in nearly back-scattering Faraday geometry. The collected light was dispersed with a single grating spectrometer (spectral resolution  $\Delta\lambda = 0.07$  nm) equipped with nitrogen cooled CCD detector and band pass filters were used to reject the stray light.

### 3. Magneto-Raman scattering of exfoliated multilayer graphene specimen

In order to obtain further information concerning our multilayer graphene sample, we have performed magneto-Raman scattering experiments in the G-band range of energy. The G-band feature of the Raman scattering spectrum is observable in the crossed

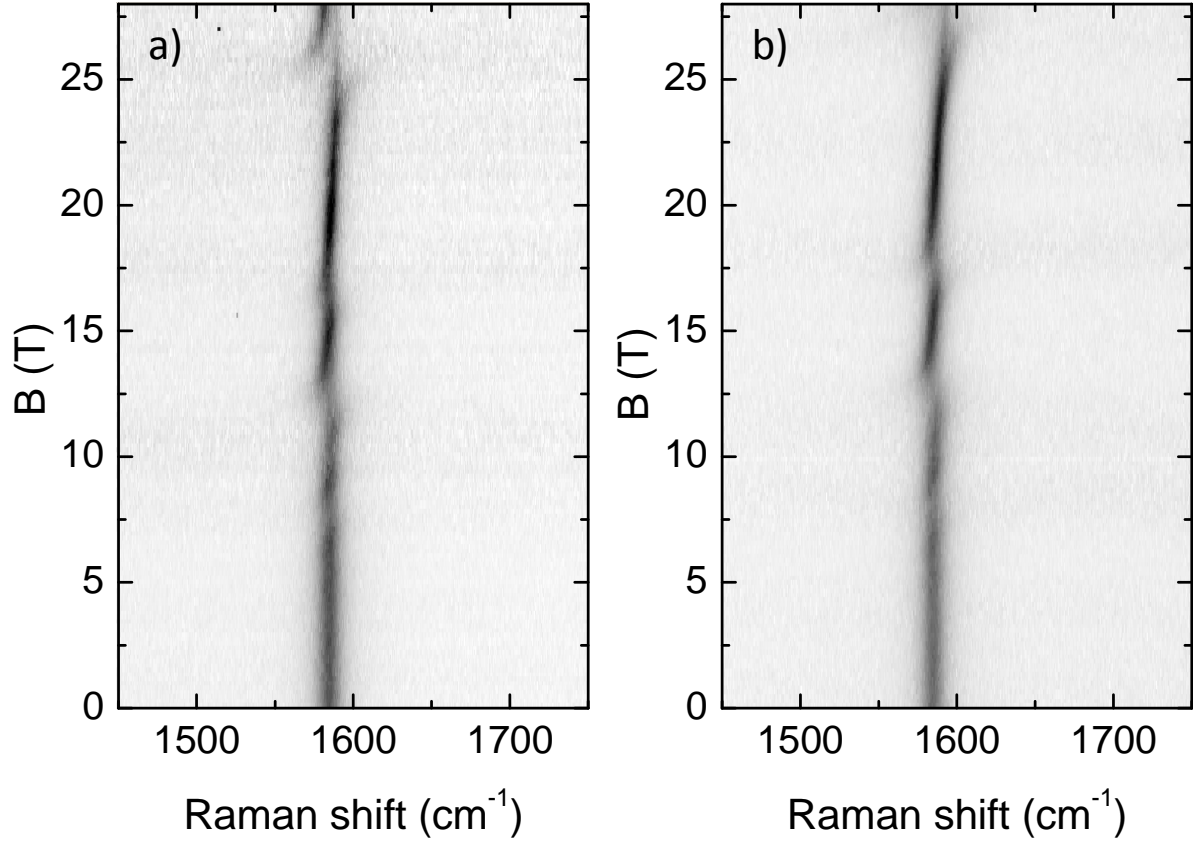


**Figure 3.** False color map of the scattered intensity in the energy range of the  $E_{2g}$  phonon as a function of the magnetic field in the  $\sigma^-/\sigma^+$  (a) and  $\sigma^+/\sigma^-$  (b) polarization configurations.

circular polarization configuration [6] which is used in the present experiment. Even though electronic excitations cannot be, in the present case, directly imaged on the Raman scattering spectra, their effect when tuned in resonance to the  $E_{2g}$  optical phonon by applying a magnetic field can be clearly observed.

The magneto-phonon resonance of our multilayer graphene sample is presented in figure 3 in the form of false color map of the scattered intensity as a function of the magnetic field, in the two crossed circular polarization configurations  $\sigma^\pm/\sigma^\mp$ . Individual spectra at characteristic values of magnetic field in  $\sigma^-/\sigma^+$  configuration are presented in figure 4a. In both configurations, we observe, for  $B > 7$  T, oscillations of the energy of the  $E_{2g}$  phonon and of its line width. This low value of the magnetic field for the onset of magneto-oscillations is an indication that the carrier density in this sample is lower than half of the  $E_{2g}$  phonon energy. The resonant values of the magnetic field are different in the two polarization configurations,  $B_{res} = 7, \mathbf{7.85}, 10, \mathbf{11.9}, 16.75, 26.6$  T in the  $\sigma^+/\sigma^-$  configuration and  $B_{res} = 6.7, \mathbf{7.3}, 9.7, \mathbf{11.4}, 15.7, 25.6$  T in the  $\sigma^-/\sigma^+$  configuration. Moreover, the electron-phonon coupling appears to be more efficient at particular values of the magnetic field (indicated above by the bold typeface) where the amplitude of the observed oscillation is enhanced with respect to other resonant

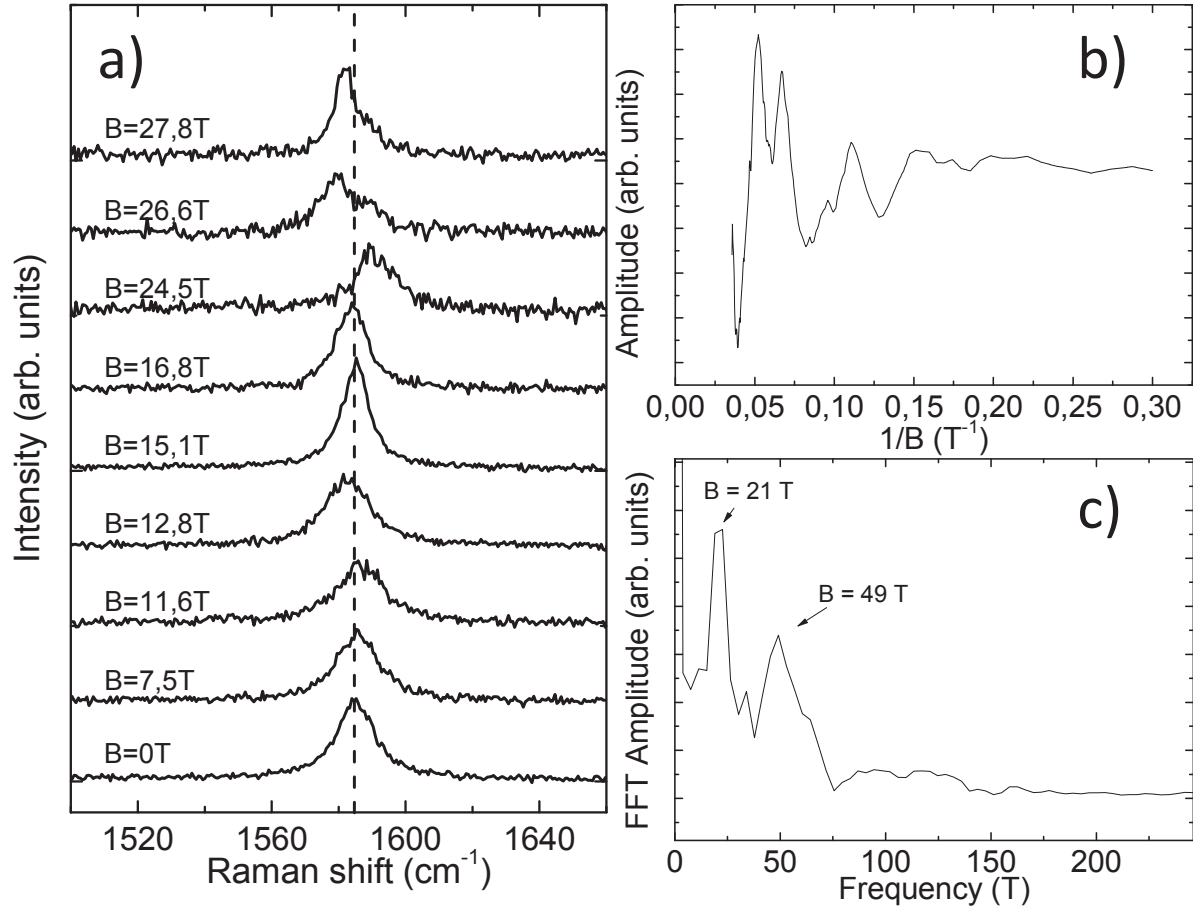


**Figure 4.** a) Raman scattering spectra measured in the  $\sigma^-/\sigma^+$  polarization configuration at different values of the magnetic field. The dashed vertical line indicates the  $B=0$  energy of the  $E_{2g}$  phonon. b) Intensity of the scattered light at the phonon energy at  $B=0$  as a function  $1/B$ . c) Amplitude of the Fourier transform of b) showing two characteristic frequencies.

magnetic fields. This nontrivial behavior is different from the one observed for epitaxial graphene, for graphene-like domains on the surface of bulk graphite or for K-point carriers in bulk graphite, where the amplitude of the oscillations was found to increase with the magnetic field as the effective electron-phonon coupling strength depends on the degeneracy of the Landau levels which increases linearly with  $B$ .

To determine the number of Landau level fan charts contributing to the observed magneto-phonon resonance, we extract from the spectra presented in figure 3a and in figure 4a the evolution of the amplitude of the scattered light at the phonon energy at  $B = 0$  as a function of the inverse magnetic field. This quantity shows oscillations which are representative of the phonon oscillations: each time the phonon feature splits or is shifted due to the resonant interaction with an electronic excitation, the amplitude of the scattered light at the phonon energy at  $B = 0$  decreases. This evolution is presented in figure 4b. It is then possible to numerically calculate the Fourier transform of this signal, presented in figure 4c, which shows two distinct frequencies at about 21 and

49 T, corresponding to two periods  $\Delta(1/B)$  of about  $0.05 \text{ T}^{-1}$  and  $0.02 \text{ T}^{-1}$ .

Their appearance can be understood qualitatively using the results of Ref. [11] for the electronic spectrum of a  $N$ -layer graphene. Namely, the spectrum is similar to that of a bulk graphite, but instead of the continuous quantum number  $k_z$ ,  $-\pi/2 < k_z \leq \pi/2$  (the wave vector, perpendicular to the layers, in the units of the inverse interlayer spacing), only  $N/2$  (for  $N$  even) or  $(N+1)/2$  (for  $N$  odd) discrete values,  $k_z = \pi/(N+1), \dots, (N/2)\pi/(N+1)$  or  $k_z = \pi/(N+1), 2\pi/(N+1), \dots, \pi/2$ , respectively, are allowed. Now, instead of a continuum of inter-Landau-level excitations for all  $k_z$  in graphite, which couple to the phonon [7], in the 4-layer graphene one has two series of inter-Landau-level excitations, corresponding to the two allowed values of  $k_z$ . Thus, the presence of two periods indicated that our sample has either three or four layers.

In the two-band approximation for the effective bilayer model of Ref. [11], the values of the magnetic field  $B_n$  at which the magnetophonon resonance occurs, are determined by

$$\left( \sqrt{n(n-1)} + \sqrt{n(n+1)} \right) \frac{v_F^2 e B_n}{\gamma_1 \cos k_z} = \omega_{\text{ph}}, \quad (1)$$

where  $v_F$  is the Fermi velocity in the monolayer, and  $\gamma_1$  is the nearest-neighbor inter-layer matrix element. Approximating  $\sqrt{n(n \pm 1)} \approx n \pm 1/2$ , we obtain

$$\frac{1}{B_n} = \frac{2v_F^2 e}{\omega_{\text{ph}} \gamma_1 \cos k_z} n. \quad (2)$$

The coefficient in front of  $n$  thus gives the period  $\Delta(1/B)$  for each value of  $k_z$ . For the monolayer-type spectrum at  $k_z = \pi/2$ , the same consideration (again, approximating  $\sqrt{n(n \pm 1)} \approx n \pm 1/2$ ) gives

$$\frac{1}{B_n} = \frac{8v_F^2 (e/c)}{\omega_{\text{ph}}^2} (n + 1/2). \quad (3)$$

For  $\omega_{\text{ph}} = 196 \text{ meV}$  and  $v_F = 1.01 \times 10^6 \text{ m/s}$  solving this equation brings an inverse period of 7.1 T, which is too small compared to the smallest observed 21 T. Thus, we exclude the possibility that our sample could be a trilayer graphene. For four layers, we have  $k_z = \pi/5, 2\pi/5$ , which, for  $\gamma_1 = 380 \text{ meV}$ , gives two frequencies of 16 and 41 T. This is an indication that the sample has four layers.

To give more solid arguments, we perform a quantitative modelling of the spectra. The Raman scattering spectra presented in figure 4 can be described by Lorentzian functions to extract the energy corresponding to the maximum of scattered light and the full width at half maximum (FWHM) of the phonon feature. These results are presented by the black dots in figure 5 (a-d) for both polarization configurations. Again, the observed behavior is not a simple series of oscillations; rather, two series of oscillations can be distinguished. Qualitatively, this is explained by the same arguments as above (two allowed values of  $k_z$ ). The theoretical curves are shown in figure. 5 as solid curves on top of the experimental symbols.

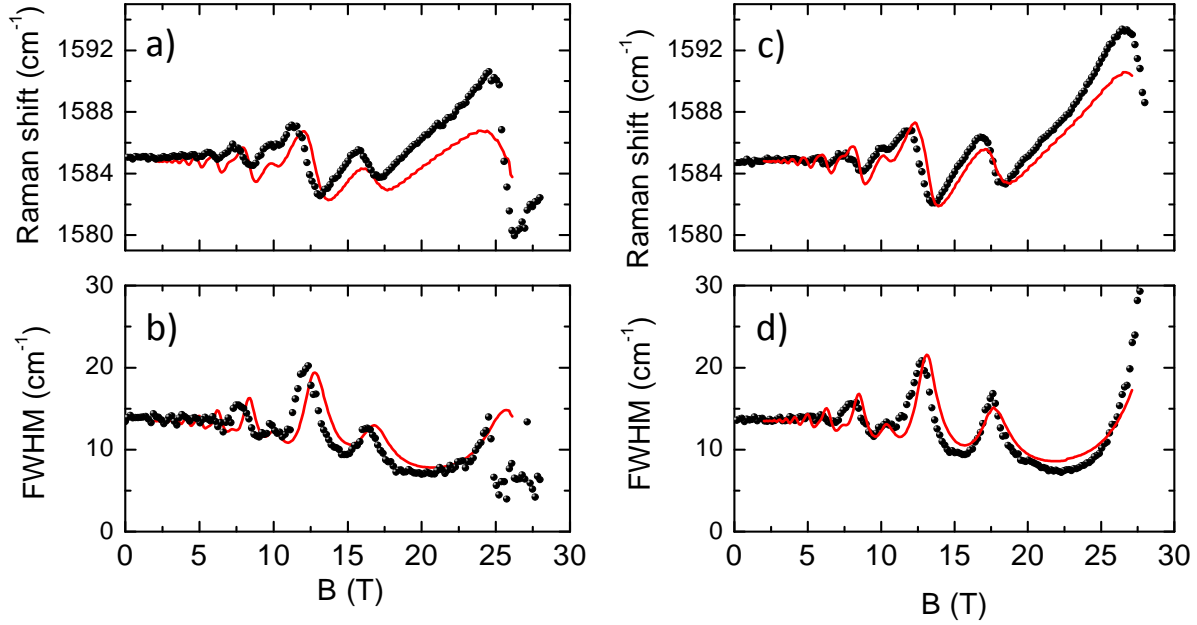


**Figure 5.** Evolution of the maximum of scattered light and of the FWHM of the G band as a function of the magnetic field in the  $\sigma^-/\sigma^+$  (a and b) and in the  $\sigma^+/\sigma^-$  polarization configurations. Red solid lines are the result of the calculation detailed in the text.

#### 4. Theoretical aspects of the magneto-phonon resonance in 4-layer graphene

In contrast to bulk graphite, where due to the translational invariance in the  $z$  direction, the momentum conservation holds, which implies that only phonons with the wave vector  $q_z = 0$  are probed (assuming the photon momentum to be very small), and that the electronic transitions involved are those from states with some  $k_z$  into states with  $k'_z = k_z - q_z = k_z$ , the 4-layer graphene lacks the translational invariance in the  $z$  direction, which introduces some additional difficulties in the theoretical description of the magneto-phonon resonance, as compared to the bulk graphite.

(i) There is *a priori* no reason to focus on one particular phonon mode. In total, there are eight degenerate optical phonon modes with zero in-plane wave vector (two for each layer). The circular basis for the in-plane polarizations is still a good one, thus for each circular polarization there are four phonon modes. We assume that their degeneracy is lifted by the electron-phonon interaction, neglecting the elastic coupling between the layers. Thus, for each of the two circular polarizations, the normal modes should be found as eigenvectors of the electronic polarization operator  $\Pi(\omega)$ , which is a  $4 \times 4$  matrix.

(ii) The electronic polarization operator not only has a contribution from the  $k_z$ -diagonal electronic transitions, but also from transitions between states with different  $k_z$ , since no momentum conservation holds. This gives not just two series of transitions, but four, corresponding to all possible combinations of  $\{\pi/5, 2\pi/5\} \rightarrow \{\pi/5, 2\pi/5\}$ .



Still, it can be naturally expected (and is confirmed by the actual calculation) that the overlap between states with different  $k_z$  is much smaller than that between states with the same  $k_z$ ; this is why two series of oscillations instead of four are seen in figure 4.

(iii) Generally speaking, all four phonon modes should contribute to the Raman spectrum. The intensities of the four components are determined by the projections of the corresponding mode eigenvectors on the Raman matrix element (photon-photon-phonon vertex), which is also a four-component vector for each given circular polarization configuration. In bulk graphite, due to the momentum conservation, the Raman vertex would be simply proportional to a  $\delta(q_z)$ , but in the 4-layer sample it has a non-trivial structure.

The electronic band structure of multilayer graphene is modelled similarly to Koshino and Ando [11]. Namely, in the nearest-layer tight-binding approximation, the band structure of any Bernal-stacked multi-layer graphene can be deduced from the one of the bulk graphite by selecting specific values of  $k_z$  corresponding to the possible standing waves perpendicular to the basal plane of the multilayer graphene specimen. The monolayer graphene then corresponds to a single value of  $k_z = \pi/2$ , the bilayer to  $k_z = \pi/3$ , the trilayer corresponds to two values of  $k_z = \pi/4, \pi/2$ , etc. At each value of  $k_z$ , the Hamiltonian has the form of an effective graphene bilayer:

$$H_{k_z}(\hat{p}) = \begin{bmatrix} \Gamma_2 & v_F \hat{p}_- & -\alpha_4 v_F \hat{p}_- & 0 \\ v_F \hat{p}_+ & \Gamma_5 & \Gamma_1 & -\alpha_4 v_F \hat{p}_- \\ -\alpha_4 v_F \hat{p}_+ & \Gamma_1 & \Gamma_5 & v_F \hat{p}_- \\ 0 & -\alpha_4 v_F \hat{p}_+ & v_F \hat{p}_+ & \Gamma_2 \end{bmatrix}, \quad (4)$$

where

$$v_F = \frac{3}{2} \frac{\gamma_0 a}{\hbar}, \quad \Gamma_1 = 2\gamma_1 \mathcal{C}, \quad \Gamma_2 = 2\gamma_2 \mathcal{C}^2, \quad \alpha_4 = \frac{2\gamma_4}{\gamma_0} \mathcal{C}, \quad \Gamma_5 = 2\gamma_5 \mathcal{C}^2 + \Delta, \quad (5)$$

$\mathcal{C} \equiv \cos k_z$ ,  $a = 1.42 \text{ \AA}$  is the distance between the neighboring carbon atoms in the same layer,  $\hat{p}_\pm = -i\hbar(\partial_x \pm i\partial_y)$  are the in-plane momenta counted from the corners of the hexagonal first Brillouin zone, and  $\gamma_0 = 3.1 \text{ eV}$ ,  $\gamma_1 = 0.38 \text{ eV}$ ,  $\gamma_2 = -20 \text{ meV}$ ,  $\gamma_4 = 44 \text{ meV}$ ,  $\gamma_5 = 94 \text{ meV}$ ,  $\Delta = -8 \text{ meV}$  are the parameters of the tight-binding Slonczewski-Weiss-McClure (SWM) model [15, 16], whose values we take the same as in Ref. [7]. As in Ref. [7], we have neglected the  $\gamma_3$  term, responsible for the trigonal warping, in order to simplify the diagonalization of the electronic Hamiltonian with an external magnetic field. The  $\gamma_2, \gamma_5$  terms in the SWM model correspond to the second-nearest-layer coupling, and their non zero values modify the electronic wave functions on the layers with respect to the simple recipe of Ref. [11]. Here, we consider the wave functions of Ref. [11] but we still include the  $\gamma_2$  and  $\gamma_5$  terms in Eq. (4), since the experimental transition energies are better reproduced when also considering these terms. Thus, even though Eq. (4), strictly speaking, does not correspond to the SWM model, we use it as an effective electronic Hamiltonian for the 4-layer graphene. Given Eq. (4), the calculation of the polarization operator is analogous to the one presented in Ref. [7] with summation over  $k_z, k'_z$  instead of integration over  $k_z$ . Following points

(i) and (ii) discussed at the beginning of this section, we also introduce a layer index for the electron-phonon coupling. The solid curves presented in figure. 5 were obtained using the values  $\lambda = 4 \times 10^{-3}$ ,  $\delta = 100$  meV for the dimensionless electron-phonon coupling constant and the electronic broadening respectively, but the values  $\lambda = 3 \times 10^{-3}$ ,  $\delta = 80$  meV or  $\lambda = 5 \times 10^{-3}$ ,  $\delta = 120$  meV differ very little. (We remind that the main purpose of the present modelling is not to extract precise values of parameters but to demonstrate that the sample is quadri-layer graphene.)

The third difficulty, mentioned at the beginning of this section, can be bypassed since we are interested only in the positions and widths of the Raman peaks, determined by the complex eigenvalues of the electronic polarization operator  $\Pi(\omega)$ , i. e., by the complex roots of the equation

$$\det [\omega^2 - \omega_0^2 - 2\omega_0\Pi(\omega)] = 0, \quad (6)$$

and not in their intensities. Moreover, it turns out that the four eigenvalues behave quite differently upon varying the magnetic field. Only one eigenvalue exhibits pronounced magneto-oscillations, while other three remain close to the bare phonon frequency. This behavior can be understood by noting that near each resonance  $\alpha$ , the polarization operator can be approximated as  $\Pi_{ij}(\omega) \sim v_i^\alpha (v_j^\alpha)^* / (\omega - \omega_\alpha + i\Gamma_\alpha)$ , where  $\omega_\alpha$  and  $\Gamma_\alpha$  are the frequency and the broadening of the corresponding transition, and  $v_i^\alpha$  is the corresponding matrix element of the electron-phonon coupling (the indices  $i, j = 1, 2, 3, 4$  label the layers where the phonon displacements occur). Then, near the resonance, one phonon eigenvector is along  $v_i^\alpha$ , and other three are orthogonal to it, so that they are effectively decoupled from the resonance. The theoretical curves in figure 5 correspond to the eigenvalue exhibiting the non-trivial oscillating behavior. Nevertheless, the contribution of other modes, not subject to oscillations, can also be distinguished in the spectrum of Fig. 3a) around the strongest resonance at  $B = 25$  T. Finally, we note that the possibility to avoid the calculation of the Raman matrix element in the 4-layer structure is quite fortunate, since its calculation requires a significant effort even in the monolayer graphene [17].

## 5. Conclusions

We have shown that magneto-phonon resonance in multi-layer graphene specimens can be used to determine the specific band structure of these systems. We demonstrate this possibility in this work with a 4-layer graphene flake deposited on SiO<sub>2</sub>. Magneto-phonon resonance in this sample result in a series of oscillations of the phonon energy which can be directly related to resonances between two distinct Landau Levels fan charts, characteristic of the 4-layer graphene system.

## Acknowledgments

Part of this work has been supported by EC MTKD-CT-2005-029671, EuroMagNET II under the EU contract number 228043 and PICS-4340 projects. P.K. is financially

supported by the EU under FP7, contract no. 221515 ‘MOCNA’.

## References

- [1] Ando T 2007 *J. Phys. Soc. Jpn.* **76** 024712
- [2] Goerbig MO, Fuch JN, Kechedzhi K and Fal’ko V 2007 *Phys. Rev. Lett.* **99** 087402
- [3] Ando T 2007 *J. Phys. Soc. Jpn.* **76** 104711
- [4] Faugeras C, Amado M, Kossacki P, Orlita M, Sprinkle M, Berger C, De Heer WA and Potemski M 2009 *Phys. Rev. Lett.* **103** 186803
- [5] Yan J, Goler S, Rhone TD, Han M, He R, Kim P, Pellegrini V and Pinczuk A 2010 *Phys. Rev. Lett.* **105** 227401
- [6] Faugeras C, Amado M, Kossacki P, Orlita M, Kühne M, Nicolet AAL, Latyshev YI and Potemski M 2011 *Phys. Rev. Lett.* **107** 036807
- [7] Kossacki P, Faugeras C, Kühne M, Nicolet AAL, Orlita M, Schneider JM, Basko DM, Latyshev YI and Potemski M 2011 *Phys. Rev. B* **84** 235138
- [8] Kim Y, Ma Y, Imambekov A, Kalugin NG, Lombardo A, Ferrari AC, Kono J, Smirnov D 2012 *Phys. Rev. B* **85** 121403(R)
- [9] Kohn W 1959 *Phys. Rev.* **2** 393
- [10] Piscanec S, Lazzeri M, Mauri F, Ferrari AC, Robertson J 2004 *Phys. Rev. Lett.* **93** 185503
- [11] Koshino M and Ando T 2008 *Phys. Rev. B* **77** 115313
- [12] Ferrari AC, Meyer JC, Scardaci V, Casiraghi C, Lazzeri M, Mauri F, Piscanec S, Jiang D, Novoselov KS, Roth S and Geim AK 2006 *Phys. Rev. Lett.* **97** 187401
- [13] Graf D, Molitor F and Ensslin K, Stampfer C, Jungen A, Hierold C and Wirtz L 2007 *Nano Lett.* **7** 238
- [14] Lui CH, Li Z, Chen Z, Klimov PV, Brus LE and Heinz TF 2011 *Nano Lett.* **11** 164
- [15] Slonczewski JC and Weiss PR 1958 *Phys. Rev.* **109** 272
- [16] McClure JW 1956 *Phys. Rev.* **104** 666
- [17] Basko DM 2009 *New J. Phys.* **11** 095011